Patch-Antenna-Based Structural Strain Measurement Using Optimized Energy Detection Algorithm Applied on USRP

Guo Chun Wan, *Member, IEEE*, Meng Meng Li, Yu Lu Yang, Liyu Xie, *Member, IEEE*, and Lan Chen

***Abstract*—A new structural health monitoring (SHM) program using spectrum sensing and radio-frequency identification technology is presented to measure structural strain. The proposed program involving universal software radio peripheral (USRP) provides an economical alternative to these type of measurements as compared to high-end equipment while this method can achieve more flexible data processing. The overall system for strain detection consists of three main parts: 1) a patch antenna as the sensor for strain; 2) an USRP as a measuring instrument; 3) a computer for data processing. The patch antenna can be used to measure structural strain by interrogating resonant frequency shift due to changes in antenna length. In this article we use the optimized energy detection algorithm applied on USRP to detect the spectrum of the patch antenna, the final measurement results show that the patch antenna sensor has a strain sensitivity 1.7678 kHz/$\mu\varepsilon$ while the error between the measured value and the true value of the stress is 2.443% after corrected by machine learning.**

***Index Terms*—Energy detection, machine learning, strain measurement, universal software radio peripheral (USRP).**

I. Introduction

STRUCTURAL health monitoring (SHM) is the integration of sensor technologies and the Internet of Things (IoT) to implement automatic detection systems of structural damages on mechanical and civil infrastructures [1]–[3]. Real-time SHM is becoming more and more important to ensure the safe and reliable operation of large structures, such as aircraft, hydroelectric power stations, dams, bridges, steel buildings and skyscrapers. The modern trend is to use wireless sensor systems in SHM to avoid high installation costs and the inconveniences inherent to wired sensor systems [4]. If the antenna is tightly fixed on the structure to be monitored, the strain on the structure will be transferred to the antenna, which then changes its dimensions and hereby its resonant frequency. Therefore, the strain state of the radio-frequency identification (RFID) patch antenna can be calculated by using RF excitation to detect the changes in the characteristic parameters of the RFID antenna. Using RFID patch antenna as a strain sensor for SHM can overcome the shortcomings of traditional detection methods, such as complicated wiring, difficulties in data transmission and analysis, and poor flexibility. As a new type of strain sensor, RFID patch antenna plays an important role in the strain sensor and has a good application prospect in the field of SHM. The RFID patch antenna can be used not only as a transmitting and receiving unit for wireless transmission of electromagnetic waves but also as a sensing unit for strain. Moreover, the sensor can be passive, wireless, and it is portable, simple, cheap, and reliable [4]–[6].

In 2002, Mita *et al.* designed a simple and low-cost passive strain sensor [5]–[7] which can monitor the peak displacement of key components. In 2004, Damiano and Timothy proved that the deformation of the RFID tag will cause changes in its backscattering intensity. According to this principle, a method for wirelessly measuring deformation of a target object is obtained. Then, a design of tag antennas with RFID chips applied to wireless strain sensors was proposed and discussed [8]. Occhiuzzi *et al.* [9] proposed and designed a strain sensor based on a folded RFID antenna in 2011. The limitation of this method is that the structure of the antenna proposed and the parameters to be detected are complicated, therefore, other changes besides the change of the strain may cause interference in the power of antenna, which also affect the parameters, such as the impedance and gain of the antenna. Due to the excessive influence factors, it is difficult to verify the exact relationship between the characteristic parameters of antenna and the magnitude of strain. Virkki *et al.* [10] used flexible textiles as the dielectric substrate for RFID antennas and studied their reliability in 2017. As far as the current research situation is concerned, many scholars focus on verifying the feasibility of using RFID patch antennas as strain sensors and use the vector network analyzer and other instruments to measure the drift of the resonant frequency, trying to explore the approximate linear relationship between resonant frequency and the magnitude of strain, there are few researches on detection methods.

In this article, we verify the feasibility of using the RFID patch antenna as a strain sensor. Then, depending on the

Manuscript received May 4, 2020; revised August 9, 2020 and September 27, 2020; accepted November 12, 2020. Date of publication November 19, 2020; date of current version April 23, 2021. This work was supported in part by the National Natural Science Foundation of China under Project 61671328; and in part by the Fundamental Research Funds for the Central Universities under Project 22120170153. *(Corresponding author: Lan Chen.)*

Guo Chun Wan, Meng Meng Li, and Yu Lu Yang are with the School of Microelectronics Science and Engineering, Tongji University, Shanghai 200092, China (e-mail: wanguochun@tongji.edu.cn; 1832943@tongji.edu.cn; 1930817@tongji.edu.cn).

Liyu Xie is with the College of Civil Engineering, Tongji University, Shanghai 200092, China (e-mail: liyuxie@tongji.edu.cn).

Lan Chen is with the School of Electrical and Electronic Engineering, Shanghai Institute of Technology, Shanghai 201418, China (e-mail: chenlan@sit.edu.cn).

Digital Object Identifier 10.1109/JIOT.2020.3039277

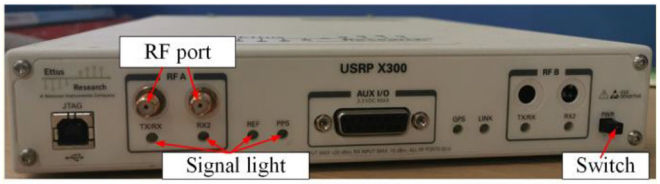

Fig. 1. Front panel of the USRP-X300.

nature that the resonant frequency of patch antenna varies with its dimension, an intelligent detection method for extracting corresponding dynamic characteristic parameters is proposed based on software radio technology and implemented on universal software radio peripheral (USRP) devices. This method improves many problems in traditional detection methods. We have demonstrated the unique advantages of the method, including simple configuration, strong robustness, wireless interrogation, etc. The USRP used in this article is X300.

Ettus Research's USRP X300 is a high-performance, scalable software-defined radio platform for designing and deploying next-generation wireless communication systems. USRP X300 is shown in Fig. 1.

It has two RF ports: 1) Ethernet port and 2) MIMO expansion port. The USRP hardware is divided into two parts: 1) the mother board and 2) the daughter board. The mother board provides basic functionalities, such as analog-to-digital converter (ADC), digital-to-analog converter (DAC), clock, and power regulation. The hardware architecture combines two extended bandwidth daughterboard slots to accommodate two daughter boards with processing frequencies covering 0–6 GHz and processing bandwidths up to 160 MHz. There are also several high-speed interface options: PCIe, 10G port, and gigabit port. The core part is a resource-rich, user-programmable Kintex-7 FPGA with 320 000 logic cells, 16M memory, and 840 multipliers. Its clock frequency reaches 200 MHz, and the stream bandwidth of each channel reaches 200 MS/s, providing high-speed connections for internal components, such as RF front-end, host interface, and DDR3 memory.

II. Spectrum Sensing and Antenna Design

The detection method proposed in this article can be divided into three steps. First, the sweep excitation signal is transmitted by the broadband antenna of USRP X300 software radio platform. Second, after the excitation signal reaches the patch antenna, it is reflected to generate an echo signal which is also received by the broadband antenna. Third, the echo signal is sampled, Fourier transformed, etc., and then the energy detection algorithm is used for signal detection. Finally, the echo signal received is divided by the excitation signal to obtain the spectrum sensing results of the patch antenna. The detailed flow chart is shown in Fig. 2.

GNU Radio is an opensource platform based on software-defined radio concepts. It is mainly used for the modeling and simulation of communication links. GNU Radio uses a two-stage design with separate data channels and control channels. C++ is used to describe signal processing modules

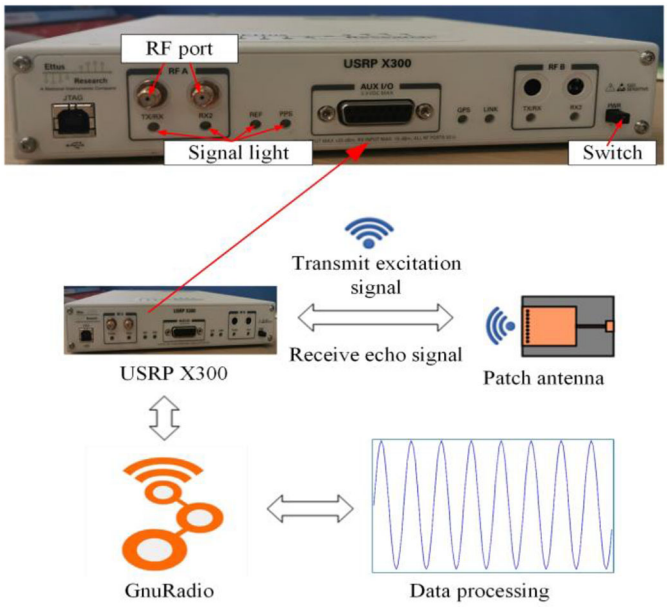

Fig. 2. Flow chart of the dynamic detection method.

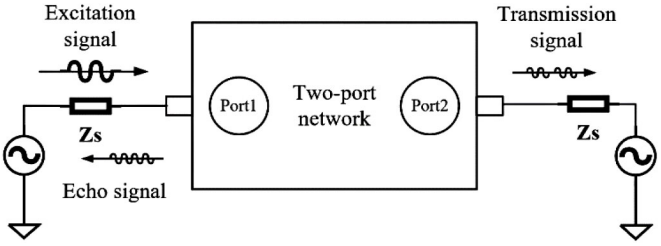

Fig. 3. Relationship between the excitation signal and echo signal.

that require higher operating efficiency and Python is used to configure and connect modules. Therefore, USRP is a flexible system that can complete wireless services through description language [11]. One of the key application technologies of software radio is spectrum sensing, which allows software radio to monitor the spectrum utilization of the surrounding environment [12].

A. Analysis of Transmit Link

The detection method based on frequency sweep measurement is actually obtained the spectrum sensing results by calculating the ratio of echo signal to excitation signal as shown in Fig. 3. Therefore, USRP is used as a signal generator to output a cosine signal as excitation signal in this article, and then the frequency of the cosine signal is continuously changed with time to generate a sweep signal whose initial frequency, end frequency, and signal power are adjustable.

The excitation signal is generated by a voltage-controlled oscillator, and the digital control unit of the USRP provides a drive voltage source to the voltage-controlled oscillator through a DAC. The oscillator generates a cosine wave of constant amplitude as the baseband waveform. The current frequency of the cosine wave depends on the amplitude of the input voltage, which is provided by the DAC. Therefore, the

frequency of the excitation signal can be controlled by the digital control unit that outputs a time-linearly increasing voltage signal through the DAC.

Due to the limitation of the hardware of USRP X300, the bandwidth of the excitation signal transmitted once is limited. Therefore, it is necessary to send a tuning command to USRP after the signal in the current frequency band is transmitted to adjust the center frequency to the next frequency point. It is known from the discussion above that the frequency of the excitation signal can be controlled by the digital control unit, which means we can transmit the excitation signal with desired starting frequency and bandwidth by adjusting digital control unit step by step.

B. Analysis of Receive Link

In the receiving link, spectrum sensing based on energy detection is used to get the echo signal of the strained patch antenna, and then the ratio of the sensing result to the excitation signal is calculated to obtain the echo loss. The first job of the signal receiving link is to sample the continuous-time-domain signal received by the Rx antenna. According to the Nyquist sampling theory, the frequency of the signal sampling must be at least twice the operating bandwidth. Suppose the target signal is $x(t)$ and its frequency range is (f_L, f_H). If $x(t)$ is sampled at a sampling rate greater than or equal to $f_S = 2(f_H\text{-}f_L)$, a time-discrete sampling signal $x(n) = x(nTs)$ can be obtained, where the sampling interval is $T_S = 1/fs$, then the signal $x(t)$ can be completely determined by the sampled signal $x(n)$. We sample the signal at the following sample rate:

$$f_s = \frac{4f_0}{2n+1} \tag{1}$$

where f_0 is the center frequency of the passband, and n is the largest positive integer that satisfies $f_S \geq 2(f_H - f_L)$. The USRP radio daughter board used in this article is CBX-120 with working frequency between 1.2 and 2.2 GHz, supporting independent operation of full-duplex TX antenna and RX antenna.

GNU Radio provides a lot of Python interfaces and functions of USRP. Therefore, the entire receive process is implemented by writing a Python program. At the same time, because of the limitation of the USB bus, the USRP X300 cannot sense the RF spectrum exceeding 8 MHz. Therefore, it is necessary to adopt a stepping method to divide the broadband spectrum that needs to be perceived into several small segments, perceiving each frequency band and then piece the results together. The entire spectrum sensing process will be described in the next section.

C. Optimization of Energy Detection Algorithm

The broadband frequency-domain energy detection algorithm is used to extract information from the received signal in this article. It is currently the most widely used spectrum sensing algorithm because it does not require any previously known characteristics of the signal in test and does not involve complex signal processing. The basic idea is to judge whether a signal exists or not by detecting the energy of the signal [13]. Signal presence detection refers to the determination of whether or not a signal exists in the frequency band after observing the signal in a certain frequency band. The basic model of this detection principle can be expressed by the following equation:

$$y[n] = \begin{cases} w[n] : H_0 \\ s[n] + w[n] : H_1 \end{cases} n = 1, ..., N \tag{2}$$

where $y[n]$ is signal sequence received by USRP, $s[n]$ signifies the signal transferred from source, $w[n]$ is the additive white Gaussian noise, and H_0 represents the frequency point is unoccupied and H_1 denotes occupied. Signal energy detection can be performed both in time and frequency domain. This article uses the detection method in the frequency domains. We use the fast Fourier transform (FFT) module in GNU Radio to realize the signal transformation from the time domain to frequency domain. For a series of discrete data, a method called period gram averaging method is used for signal detection. The baseband complex signal is obtained by USRP sampling first, then the sampled signal is converted into a vector, which is added with a Blackman–Harris window (the main function of windowing is to reduce side lobes and weaken spectrum leakage). Then, this method computes a fixed-bandwidth N-point FFT around the center frequency and then averages the positive values generated by the FFT. Finally, the squared value of the signal is calculated to obtain the energy of the signal. The cumulative energy T can be expressed by the following equation:

$$T = \sum_{i=1}^{N} y_i^2 = \begin{cases} \sum_{i=1}^{N} w_i^2, H_0 \\ \sum_{i=1}^{N} (s_i + w_i)^2, H_1. \end{cases} \tag{3}$$

For energy detection, the false alarm rate refers to the probability that there is no signal but the detection result is that the signal exists. We hope to effectively improve the detection rate and reduce the false alarm rate to optimize the detection effect of the system. When the number of sampling points N is large enough, both $w[n]$ and $s[n]$ obey the Gaussian distribution, and their mean and variance are 0 and ${\sigma_n}^2$, 0 and ${\sigma_s}^2$, respectively. The target detection rate (P_d) and target false alarm rate (P_f) can be expressed as the following equations, respectively:

$$P_d = P(T > \lambda | H_1) = Q\left(\frac{\lambda - N(\sigma_n^2 + \sigma_s^2)}{\sqrt{2N(\sigma_n^2 + \sigma_s^2)^2}}\right) \tag{4}$$

$$P_f = P(T > \lambda | H_0) = Q_N\left(\frac{\lambda - N\sigma_n^2}{\sqrt{2N\sigma_n^4}}\right) \tag{5}$$

where Q_N is the complementary distribution function of the standard Gaussian, and λ is a predetermined threshold for energy detection

$$Q_N = \frac{1}{\sqrt{2\pi}} \int_x^{\infty} \exp(\frac{-y^2}{2}) dy. \tag{6}$$

In practical applications, the target false alarm rate will increase with the target detection rate; on the other hand, if the target detection rate is too low, it will result in the loss of

existing signals. Therefore, it is necessary to select an appropriate threshold λ to balance the target false alarm rate and the target detection rate. The noise power and signal power must be known to obtain the optimal threshold λ. The noise power can be obtained by estimation, but it is necessary to know the propagation characteristics of the signal to obtain the signal power. In practical applications, the target false alarm rate is usually determined first, and a unique threshold can be calculated in the case where the false alarm rate and the signal-to-noise ratio (SNR) are determined [14], as shown in the following equation:

$$\lambda = Q^{-1}(P_f\sqrt{2N} + N)\sigma_n^2. \tag{7}$$

The main disadvantage of traditional energy detection as described above is that it cannot detect multiple signals with different SNRs in a wideband. What is more, as the SNR decreases, the computational complexity increasing rapidly and the performance deteriorates drastically. An improved relevance-based energy detection is proposed [15] to determine the specific bandwidth of signals on the premise of a high-detection rate with low-SNR signals under a fine resolution based on this result.

The relevance-based energy detection find low-SNR signals by $n1$ points out of n have a greater power than noise power. Denote this as relevance window, n as the size of the relevance window, ρ = n1/n as relevance ratio, andPs as the probability of consecutive frequency points detected as occupied by the relevance window [16]

$$P_s = \sum_{k=n1}^{n} C_n^k \times P_{T>\hat{\sigma}_w^2} \times \left(1 - P^k_{T>\hat{\sigma}_w^2}\right)^{n-k} \tag{8}$$

$$\hat{\sigma}_w^2 = \frac{(1-\eta)(1-P_f)\sigma_n^2 + \eta P_m(\sigma_n^2 + \sigma_s^2)}{(1-\eta)(1-P_f) + \eta P_m} \tag{9}$$

where P_m is the probability that an occupied frequency point's power is lower than threshold, and *?* is the occupancy rate of the signal in the frequency band, respectively.

In this article, the influence of different SNR and false alarm rate on detection effect is observed in MATLAB. First, a binary phase-shift keying (BPSK) signal is generated as the signal to be detected. The detection rate of the energy detection algorithm is calculated with different SNR and false alarm rate. The relationship between SNR, false alarm rate, and detection rate is shown in Fig. 4.

The simulation results show that both algorithms still have high-detection accuracy rate and low false alarm rate in the case of low SNR and the improved algorithm achieves a more accurate spectrum detection effect. In this article, the power of the excitation signal transmitted by the software radio is much larger than the noise signal in the air, so the SNR is relatively high so that the algorithm can obtain good detection results.

D. Antenna Design

In order to realize the wireless detection of strain dynamic characteristics of the RFID antenna by the USRP platform, it is necessary to configure the USRP X300 platform with the appropriate transceiver antenna besides adopting a reasonable energy detection algorithm.

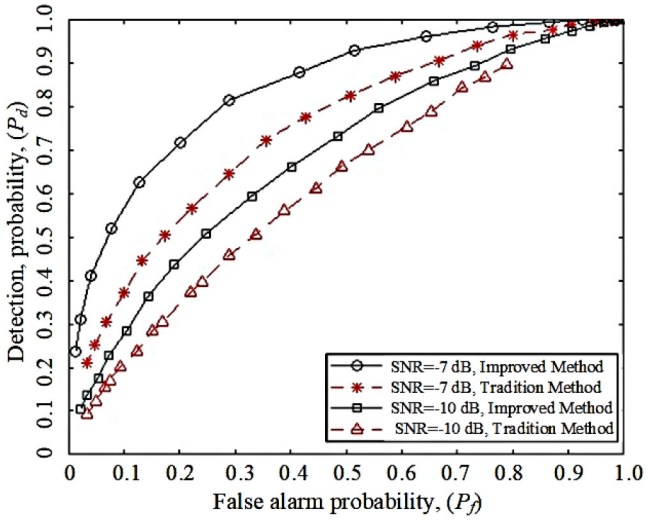

Fig. 4. Relationship between SNR and detection results.

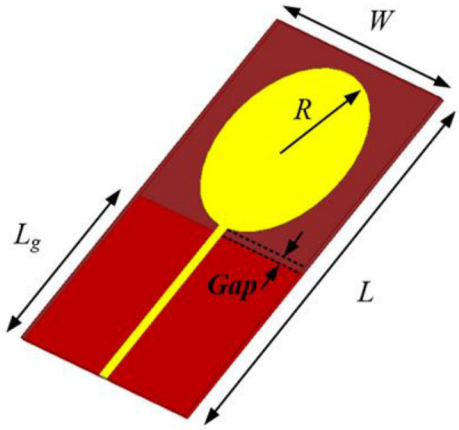

Fig. 5. Configuration of the broadband antenna.

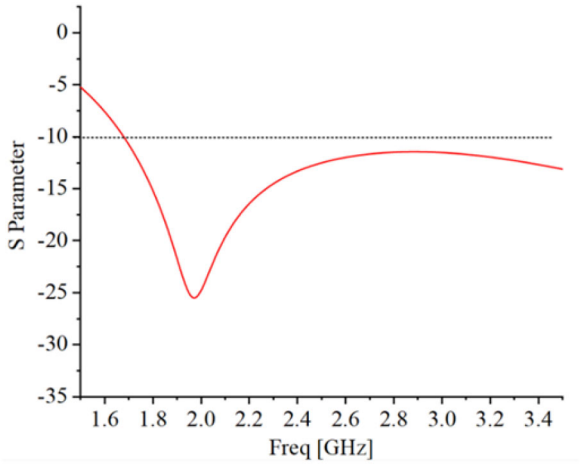

Fig. 6. Simulation result of broadband antenna.

The structure of the broadband antenna used in this article is shown in Fig. 5. The material of the dielectric substrate is F4B (ε_r = 2.33 and tanδ = 0.0015). According to the impedance formula of microstrip line, it can be concluded that the width

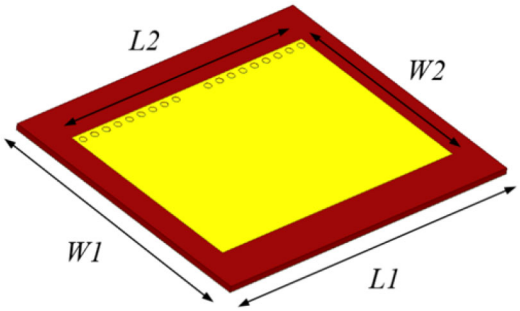

Fig. 7. Configuration of the proposed patch antenna.

TABLE I
DIMENSIONS OF THE BROADBAND ANTENNA

Parameter	W	L	R	L_g	Gap
Dimensions (mm)	45.00	66.00	16.00	30.00	1.00

of microstrip line with characteristic impedance of 50 Ω is 2.2 mm.

For detailed design, all parameters of the broadband antennas are simulated using the HFSS and are given in Table I. Fig. 6 shows that the antenna has the reflection coefficient less than −10 dB in the band 2–3 GHz. The radiation performance of the antenna is good over the whole frequency band.

The resonant frequency of patch antenna is related to its electrical length. Therefore, the resonant frequency of patch antenna will change when the physical size of antenna is changed, and the drift of frequency is linear with the stress acting on the antenna. In this article, we choose rectangular microstrip antenna as the strain patch antenna of RFID. The designed antenna is shown in Fig. 7. The initial resonant frequency (f_{re}) of the antenna is 2.396 GHz.

The vias of the patch antenna are connected between the top copper cladding and the bottom copper ground layer as shown in Fig. 7. The vias will change the boundary conditions at the end of the metal patch, which increases the electrical length of current propagation. This configuration reduces the patch antennas by half. In theory, the resonant frequency of a standard quarter wave length rectangular microstrip antenna can be calculated by the following equation:

$$f_{re} = \frac{c}{4(L + \Delta L)\sqrt{\varepsilon_{re}}} \tag{10}$$

where c is the speed of light, L is the length of the conducting patch, ε_{re} indicates the effective dielectric constant of the substrate, and ΔL is the length of compensation which is related to the width of the conducting patch W, the effective dielectric constant of the substrate ε_{re}, and the ratio of the width of the conducting patch to the thickness of the dielectric substrate W/h. The optimized antenna dimensions are depicted in Table II.

TABLE II
DIMENSIONS OF THE PATCH ANTENNA

Parameter	$W1$	$L1$	$W2$	$L2$
Dimensions (mm)	21.93	25.16	15.46	21.32

III. SIMULATION AND TENSILE EXPERIMENTS

A. Simulation of Strain Sensor

The longitudinal strain ε_L is usually defined as the relative change in the length of an object, i.e.,

$$\varepsilon_L = \frac{L_s - L_o}{L_o}. \tag{11}$$

Then, the change of resonant frequency can be estimated by the following equation [17], where K_α is a constant, we can see that the relationship between the resonant frequency and ε_L is linear.

$$f_{re}(\varepsilon_L) = \kappa_\alpha \varepsilon_L + f_{re}. \tag{12}$$

The loads are adjusted so that ten different strain levels (from 0% to 10% at an increment step of 1%) are generated in the patch antenna. In this article, the sensor dimension is simply scaled according to applied strain. After the mechanical simulation at each strain level, the lowest peak of S parameter plot is picked as the resonant frequency of the antenna under strain finally. Fig. 8 shows the simulation results.

Fig. 8(a) shows S parameter at different strain levels and the resonant frequency of the patch antenna reduces as the strain increases. Fig. 8(b) illustrates linear regression between resonant frequencies and corresponding strain levels. The value of 2.2830 means 1-$\mu\varepsilon$ increment in the base structure generates 2.2830 KHz decrease in antenna resonant frequency. The figure also shows the coefficient of determination (R^2) is 0.9997, which indicates a good linearity between resonant frequency and strain.

B. Measurement and Strain Detection

After investigating the performance of patch antenna using simulation, the strain sensor is fabricated and the simulation results are validated through experimental studies. The components of the wireless measurement environment are: anechoic chamber, aluminum sheet with patch antenna attached (pasted vertically), strain collector, stretching machine, broadband antenna, and USRP X300.

The broadband antenna and the TX/RX port of USRP are connected through the SMA adapter and the coaxial cable during the measuring period. The aluminum plate with patch antenna is tightly clamped with the clamp of the stretching machine, and then adjust the aluminum plate to maintain the level of the broadband antenna and the patch antenna. Finally, uniformly distributed tensile loads are applied at two ends of the aluminum plate, after the indicator of the strain acquisition instrument is stable, the detection algorithm proposed in this article is used for wireless detection. The experimental system for strain measurement is shown in Fig. 9.

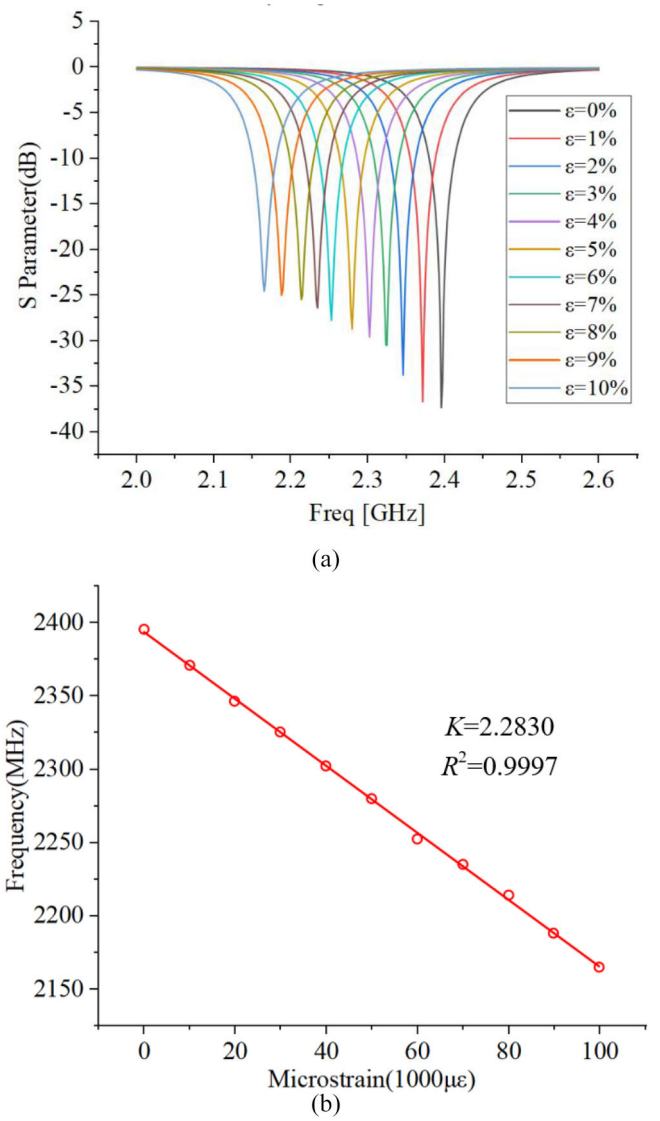

Fig. 8. (a) S11 parameters under strain transfer. (b) Resonant frequency versus strain.

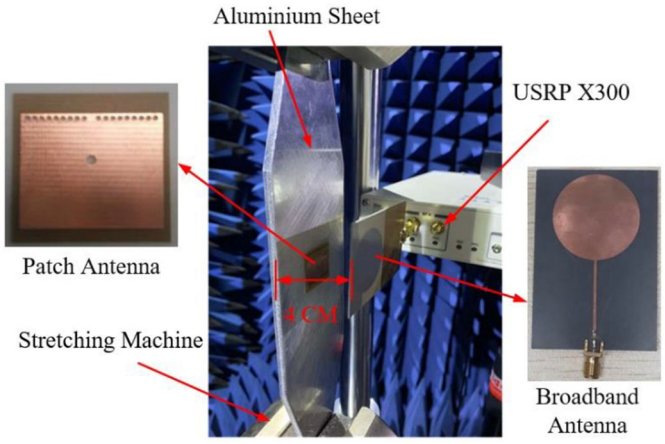

Fig. 9. Measurement setup inside anechoic chamber.

Considering the efficiency of mechanical strain transfer from the base structure to the top surface of the antenna sensor, defined as η_L [18], the relationship between the drift of the resonant frequency and the stress experienced by the sensor can be expressed as the following equations [18]:

$$F_L = \frac{EA(f_{re} - f_{re}(\varepsilon_L))}{f_{re}\eta_L} \tag{13}$$

where E and A are constants representing the modulus of elasticity and cross-sectional area, respectively. F is the stress applied to the aluminum sheet. After the initial resonant frequency of the antenna and the drift of the resonant frequency is measured by USRP, we can calculate the actual magnitude of the stress applied to the antenna by this equation.

Fig. 10 shows that the strain antenna we proposed has strong scattered power in the horizontal polarization direction, so it will produce unnecessary coupling with the broadband antenna with the same polarization. Therefore, before extracting the sample point, the measured data require extra treatment due to the presence of undesired elements. These undesired elements include: coupling between the antennas, and scattering from background objects. In order to remove these undesired components, two different measurements are required. It should be noted that we do not care about characterizing these undesired elements, but simply removing them [19].

The first measurement is done with no objects present in the plane of measurement

$$R_1 = \text{Coupling}(H_s, H_b) + \text{Background scattering}. \tag{14}$$

The second measurement is with the tag present

$$R_2 = \text{Coupling}(H_s, H_b) + \text{Background scattering Echoloos}. \tag{15}$$

The final step in processing the data is accomplished via a subtraction operation as

$$\text{Echoloos} = R_2 - R_1. \tag{16}$$

N data points obtained by USRP are used for data fitting and the lowest point is taken as the resonant frequency of the antenna after these undesired components are removed. In order to get more accurate experimental results without special circumstances, the experiment is repeated ten times and the average value is used as the final result. The results of one measurement are shown in Fig. 11.

The result shows that the resonant frequency of the antenna is 2292.8 MHz at zero stress level. Then, the resonant frequency of the deformed antenna is measured. the measured and true values of the stress applied to the antenna are calculated as shown in Fig. 12.

Then, the measured values of the stress are substituted into (13), and the strain is calculated as shown in Fig. 13.

As shown by linear regression in Fig. 13, the strain sensitivity is -1.7678k Hz/$\mu\varepsilon$, which is lower than the theoretical prediction of -2.2830 kHz/$\mu\varepsilon$. One potential reason is that in the simulation, the strain/deformation in the antenna will not only change the length of the antenna, but also the dimensions of other antenna components (including matching lines, vias, and substrates). As a result, these more complicated influences to strain sensitivity are not taken into consideration by the simplified theoretical prediction in (12).

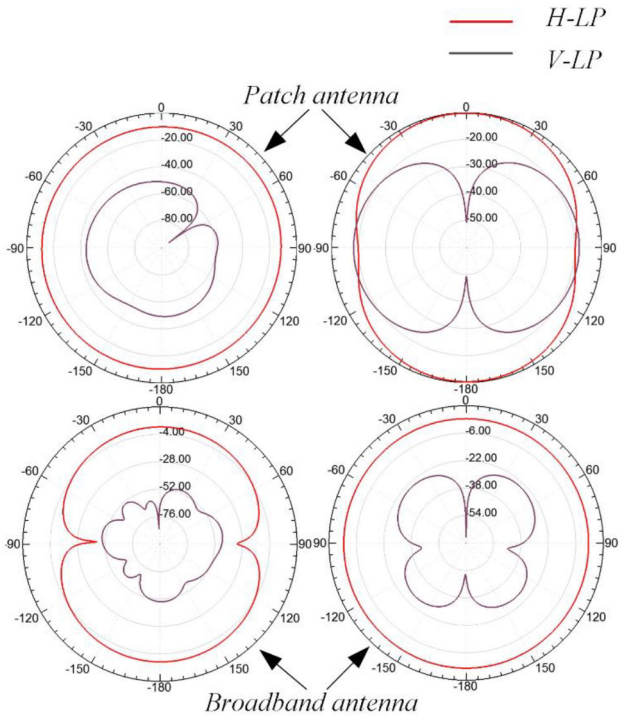

Fig. 10. Comparison of scattered power in horizontal polarization and vertical polarization.

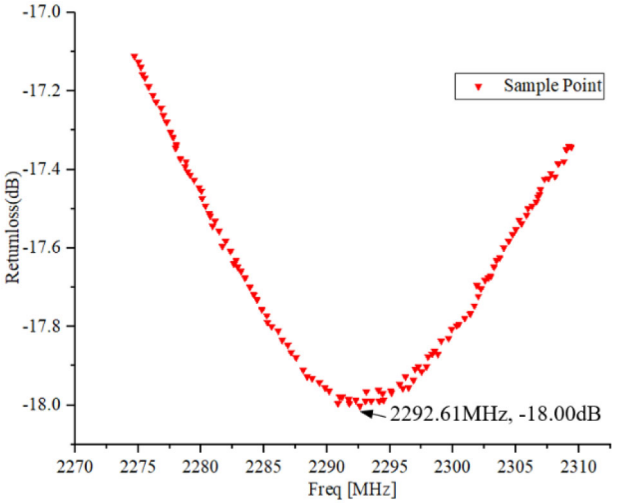

Fig. 11. Initial resonant frequency measured by USRP.

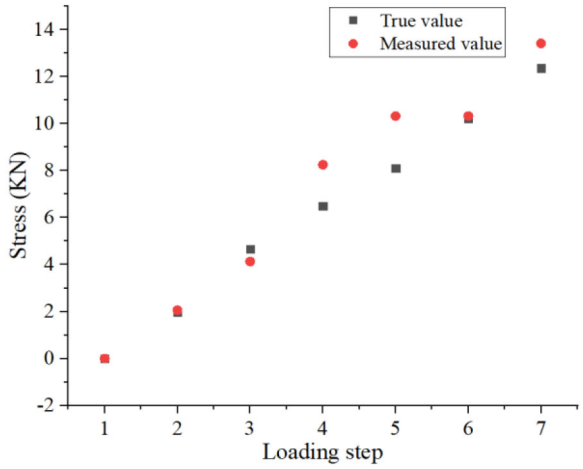

Fig. 12. Comparison of true and measured results.

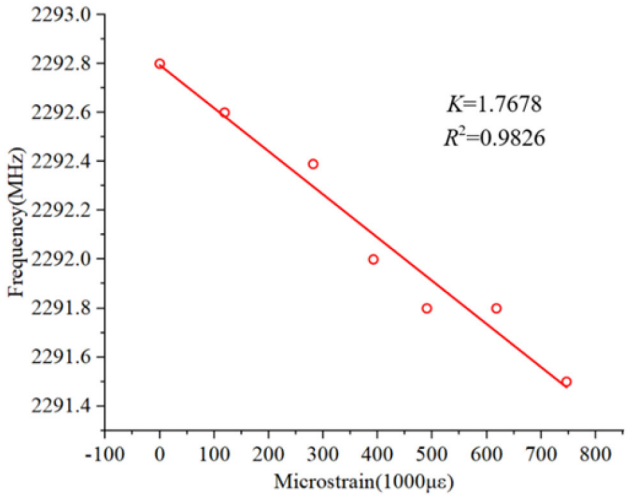

Fig. 13. Linear fitting of strain and resonant frequency.

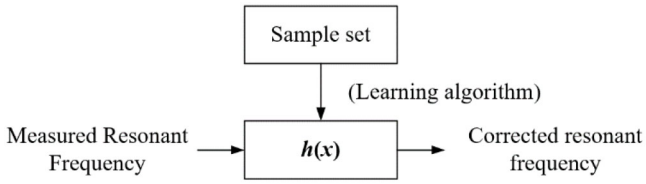

Fig. 14. Error correction machine learning algorithm.

IV. Machine Learning for Data Processing

Because the sources of errors in the wireless detection environment are complex, including the loss of electromagnetic waves in the air, the interference of the metal body and the metal collet of the stretching machine, and the resonant interference of the transmitting and receiving antennas, it is difficult to accurately analyze the error of the actual environment modeling. In order to effectively correct the error between the experiment and the theory and improve the accuracy of the detection, the machine learning method shown in Fig. 14 is used in this article.

First, the measured resonant frequency f_x of the antenna sensor is recorded, then calculate the theoretical resonant frequency f_y according to the actual stress displayed by the stretching machine and use the measured sets (f_x, f_y) as the training set to obtain a relationship model (h) between the measured resonant frequency and the theoretical resonant frequency by machine learning. The resulting relational model is actually a functional mapping from f_x to f_y, and the expression is shown in following equation:

$$h_\theta(f_x) = \theta^T f_x = \theta_0 f_{x0} + \theta_1 f_{x1} + \cdots + \theta_n f_{xn} = \sum_{i=0}^{n} \theta_i f_{xi}. \quad (17)$$

Different values of θ_i will result in different hypothesis functions. In order to obtain a more accurate hypothesis function, it is necessary to calculate the optimal θ_i so that the predicted value f_y closest to the actual value can be obtained after the input parameter f_x is input.

The parameter θ determines the error between the predicted value of the model and the actual value in the training set. Therefore, the problem is transformed into finding the optimal model parameters, so that the error can be minimized, that is, the value of the cost function formula is the smallest. The cost function formula can be expressed by the following equation, m denotes the number of instances in the training set

$$J(\theta) = \frac{1}{2m}\sum_{i=1}^{m}(h_\theta(f_x^{(i)} - f_y^{(i)}))^2. \tag{18}$$

In this article, there is only one input variable (the measured resonant frequency), therefore this is a univariate linear regression problem with a hypothetical function as

$$h_\theta(f_x) = \theta_0 + \theta_1 f_{x1}. \tag{19}$$

A gradient descent algorithm [20] was used to obtain the smallest cost function in this article. First, θ_0 and θ_1 are changed iteratively after both of them are initialized to 0 in order to make $J(\theta_0, \theta_1)$ continuously decreases. When $J(\theta_0, \theta_1)$ no longer changes, the minimum value (or local minimum value) of the cost function can be obtained. The iterative method is shown in the following:

$$\theta_j := \theta_j - \alpha\frac{1}{m}\sum_{i=1}^{m}(h_\theta(x^{(i)}) - y^{(i)})x_j^{(i)}. \tag{20}$$

The variable learning rate α is introduced into the equation to change the speed at which the value of θ changes. If α is too small, the excessive number of iterations will result in slow iterations. If α is too large, the local optimal point may be skipped or even the algorithm may not converge. We performed 67 sets of tensile measurements on the RFID strain antenna. The 67 sets of measured data and their corresponding theoretical resonance frequencies (f_x, f_y) are used as the training set, which was trained using MATLAB according to the above algorithm. The linear regression results obtained by the gradient descent method is shown in Fig. 15. There is a set of parameters that can minimize the value of the cost function, and the correction result is the best at this time. In this way, we get the optimal solution of (θ_0, θ_1) as (0.366766, 0.839853).

Substituting the measurement data of the resonant frequency into (19) will obtain the corrected resonant frequency, which can be substituted into (21) to obtain the corrected stress value as shown as follows:

$$F_L = \frac{EA(f_{re} - 0.366766 - 0.839853 \cdot f_{x1})}{f_{re}\eta_L}. \tag{21}$$

It can be known from the above discussion that the error between the measured stress and the true value is 9.8% before correction as shown in Fig. 12. The results obtained by substituting the measured stress into the correction equation (21) are shown in Fig. 16. The error between the corrected value and the true value is 2.43%. The results before and after the correction show that the corrected mathematical model is more accurate and can be used as a basis for further analysis and research.

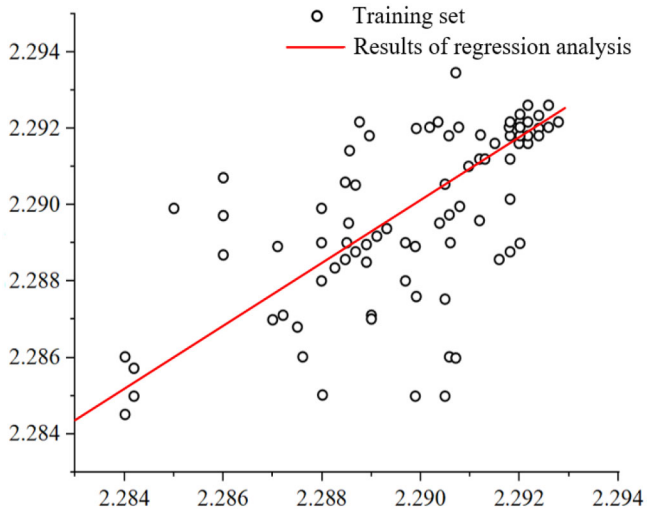

Fig. 15. Linear regression results obtained by gradient descent.

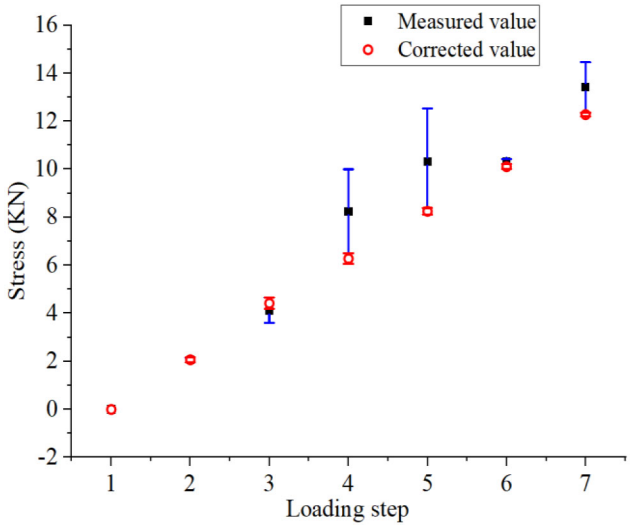

Fig. 16. Comparison of corrected and measured results.

V. Conclusion

This article demonstrated a detection program implemented on USRP. A strain detection scheme that comprises the signal transmission, signal reception, spectrum analysis, data processing is developed based on the improved energy detection algorithm which can detect multiple signals with different SNRs in a wideband. In detail, USRP is used to output a sweep signal through the broadband antenna as excitation signal, an echo signal containing strain information will be generated after the excitation signal reaches the patch antenna. Then, the echo signal reflected by the patch antenna will be detected using the improved energy detection algorithm. Finally, machine learning implemented on the PC is used to correct the error between the measured value and the true value. In the whole process, the broadband antenna, as

a key peripheral of USRP, plays the role of transmitting and receiving radio-frequency signals.

This program can realize real-time and wireless data analysis and detection. It is more intelligent and economical than traditional network analysis instrument detection methods. In the future, we will write the machine learning algorithms into USRP to achieve better integration and explore the vector parameter measurement scheme to solve the problem that the energy detection algorithm cannot measure the signal phase.

REFERENCES

[1] J. P. Lynch, C. R. Farrar, and J. E. Michaels, "Structural health monitoring: Technological advances to practical implementations [scanning the issue]," *Proc. IEEE*, vol. 104, no. 8, pp. 1508–1512, Aug. 2016.

[2] N. Dlodlo, O. Gcaba, and A. Smith, "Internet of Things technologies in smart cities," in *Proc. IST-Africa Week Conf.*, Durban, South Africa, 2016, pp. 1–7, doi: 10.1109/ISTAFRICA.2016.7530575.

[3] A. M. J. Marindra and G. Y. Tian, "Chipless RFID sensor tag for metal crack detection and characterization," *IEEE Trans. Microw. Theory Techn.*, vol. 66, no. 5, pp. 2452–2462, May 2018, doi: 10.1109/TMTT.2017.2786696.

[4] S. Xue, K. Xu, L. Xie, and G. Wan, "Crack sensor based on patch antenna fed by capacitive microstrip lines," *Smart Mater. Struct.*, vol. 28, no. 8, Jul. 2019, Art. no. 085012, doi: 10.1088/1361-665x/ab2834.

[5] A. Mita and S. Takahira, "Health monitoring of smart structures using damage index sensors," in *Proc. SPIE Int. Soc. Opt. Eng.*, vol. 4696, 2002, pp. 92–99.

[6] A. Mita, and S. Takahira, "Damage index sensor for smart structures," *Struct. Eng. Mech.*, vol. 17, nos. 3–4, pp. 331–346, Mar./Apr. 2004.

[7] A. Mita and S. Takhira, "A smart sensor using a mechanical memory for structural health monitoring of a damage-controlled building," *Smart Mater. Struct.*, vol. 12, no. 2, pp. 204–209, Apr. 2003.

[8] D. Patron, T. Kurzweg, A. Fontecchio, G. Dion, and K. R. Dandekar, "Wireless strain sensor through a flexible tag antenna employing inductively-coupled RFID microchip," in *Proc. Wireless Microw. Technol. Conf. (WAMICON)*, Tampa, FL, USA, 2014, pp. 1–3.

[9] C. Occhiuzzi, C. Paggi, and G. Marrocco, "Passive RFID strain-sensor based on meander-line antennas," *IEEE Trans. Antennas Propag.*, vol. 59, no. 12, pp. 4836–4840, Dec. 2011, doi: 10.1109/TAP.2011.2165517.

[10] J. Virkki, T. Björninen, M. Akbari, and L. Ukkonen, "Strain reliability and substrate specific features of passive UHF RFID textile tag antennas," in *Proc. IEEE Int. Conf. Electron. Circuits Syst. (ICECS)*, Monte Carlo, Monaco, 2016, pp. 404–407, doi: 10.1109/ICECS.2016.7841218.

[11] D.-J. Lee and M.-S. Jang, "Optimal spectrum sensing time considering spectrum handoff due to false alarm in cognitive radio networks," *IEEE Commun. Lett.*, vol. 13, no. 12, pp. 899–901, Dec. 2009.

[12] K. Seshukumar, R. Saravanan, and M. S. Suraj, "Spectrum sensing review in cognitive radio," in *Proc. Int. Conf. Emerg. Trends VLSI Embedded Syst. Nano Electron. Telecommun. Syst. (ICEVENT)*, Tiruvannamalai, India, 2013, pp. 1–4.

[13] V. I. Kostylev, "Energy detection of a signal with random amplitude," in *Proc. IEEE Int. Conf. Commun. ICC (Cat. No.02CH37333)*, vol. 3. New York, NY, USA, 2002, pp. 1606–1610.

[14] J. E. Salt and H. H. Nguyen, "Performance prediction for energy detection of unknown signals," *IEEE Trans. Veh. Technol.*, vol. 57, no. 6, pp. 3900–3904, Nov. 2008, doi: 10.1109/TVT.2008.921617.

[15] J. J. Lehtomaki, M. Juntti, H. Saarnisaari, and S. Koivu, "Threshold setting strategies for a quantized total power radiometer," *IEEE Signal Process. Lett.*, vol. 12, no. 11, pp. 796–799, Nov. 2005.

[16] S. Fang, P. Zuo, T. Peng, and W. Wang, "An adaptive resolution and improved relevance-based energy detection algorithm in cognitive radio," in *Proc. 4th Int. Conf. Syst. Informat. (ICSAI)*, Hangzhou, China, 2017, pp. 911–916, doi: 10.1109/ICSAI.2017.8248415.

[17] G. C. Wan, K. Xue, R. X. Gao, J. Y. Lv, and M. S. Tong, "A rectangular microstrip patch antenna used for structural health monitoring," in *Proc. IEEE Int. Symp. Antennas Propag. USNC/URSI Nat. Radio Sci. Meeting*, Boston, MA, USA, 2018, pp. 695–696.

[18] C. Wan *et al.*, "Transverse deformation effect on sensitivity of strain-sensing patch antenna," *Int. J. Distrib. Sens. Netw.*, vol. 12, no. 3, 2020, Art. no. 15501477209.

[19] A. T. Blischak and M. Manteghi, "Embedded singularity chipless RFID tags," *IEEE Trans. Antennas Propag.*, vol. 59, no. 11, pp. 3961–3968, Nov. 2011.

[20] C. Zheng and Z. Guangming, "Application on express delivery of an immune genetic algorithm based on machine learning," in *Proc. 2nd Int. Symp. Comput. Intell. Design*, Changsha, China, 2009, pp. 165–167, doi: 10.1109/ISCID.2009.189.

Guo Chun Wan (Member, IEEE) received the M.S. and Ph.D. degrees in transportation information engineering and control from Tongji University, Shanghai, China, in 2005, and 2011, respectively.

He became an Associate Professor with Tongji University in 2002. He joined the Department of Electronic Science and Technology, Tongji University in 2006. His current research interests include signal and information processing, with the emphasis on error-correcting coding, VLSI architectures, RFID strain sensor and System-on-Chip design for communications, and coding theory applications.

Meng Meng Li received the B.S. degree in electronic information engineering from Southwest Jiaotong University, Sichuan, China, in 2018. He is currently pursuing the Bachelor of Engineering degree in microelectronics science and engineering, Tongji university, Shanghai, China.

His current research interests include structural health monitoring and usrp.

Yu Lu Yang received the B.S. degree in electronic engineering and intelligent control from Shanghai Maritime University, Shanghai, China, in 2019. She is currently studying in microelectronics science and engineering, Tongji university, Shanghai, China.

Her current research interests include antenna equivalent circuit modeling and tag antenna design.

Liyu Xie (Member, IEEE) received the B.S. and M.S. degrees in mechanics engineering from Tongji University, Shanghai, China, in 2000 and 2003, respectively, and the Ph.D. degree in system design engineering from Keio University, Tokyo, Japan, in 2009.

In 2009, he started a career as an Assistant Professor with the College of Civil Engineering, Tongji University, and was promoted to an Associate Professor in 2019. He has authored or coauthored over 20 publications in international journals. His current research focuses on smart sensors, structural health monitoring, and structural vibration control.

Dr. Xie is a member of SHMII.

Lan Chen received the M.S. degree in signal and information processing from Tongji University, Shanghai, China, in 2004, and the Ph.D. degree in astronomical technology and method science from Shanghai Astronomy, Chinese Academy of Sciences, Shanghai, in 2010.

She is currently a Professor with the Shanghai Institute of Technology, Shanghai, and serves as the Associate Dean of the School of Electrical and Electronic Engineering. Her current research interests include high-speed digital signal processing, digital terminal technology research, and signal simulation technology.